Static vulnerability of an existing r.c. structure and seismic retrofitting by CFRP and base-isolation: A case study

Fabio Mazza *, Daniela Pucci

Dipartimento di Ingegneria Civile, Università della Calabria, Via P. Bucci, 87036 Rende (CS), Italy

ABSTRACT

The assessment of the static vulnerability under gravity loads of existing reinforced concrete (r.c.) framed buildings is a serious problem that requires the use of reliable methodologies to evaluate ductile and brittle mechanisms. The present work compares alternative formulations of member chord rotation and section and joint shear strength, proposed by Italian and European seismic codes and guidelines and other expressions available in the scientific literature. To this end, a r.c. framed building built sixty years ago with bi-directional (perimeter) and mono-directional (interior) plane frames, originally designed for five storeys then elevated to six during construction, is studied. A full characterization of the structure and its materials is carried out by means of destructive and non-destructive methods. Then, retrofitting based on the use of both innovative material, such as carbon fibre reinforced polymers (CFRP), and technology, such as base-isolation, are adopted to improve the static and seismic performances of the original structure. Finally, nonlinear analyses are carried out on a three-dimensional fibre model of the original and retrofitted structures, where an elastic linear law idealizes the behaviour of the CFRP up to tension failure and viscoelastic linear and bilinear models are used to idealize the behaviour of the elastomeric and sliding bearings, respectively.

© 2016 Elsevier Ltd. All rights reserved.

1. Introduction

In general, the static vulnerability of old Italian reinforced concrete (r.c.) framed buildings can be traced to degradation of the material properties, due to the effects of time and earthquakes [1], and low building standards, with insufficient attention to details and poor quality control at the time of construction [2]. The assessment of their structural weakness is complex due to a lack of effective knowledge of the structure [3] and accuracy and reliability of the capacity models available in the scientific literature for evaluating failure mechanisms, both ductile, at member level, and brittle, at section and joint levels. A lot of mechanical-empirical formulations, calibrated in accordance with experimental data, is available to evaluate ductile mechanism in terms of chord rotation capacity [4]. Moreover, brittle mechanism at section level represents a typical problem in columns of r.c. existing framed structures designed in line with out-of-date seismic codes, where capacity design criteria to avoid brittle failure modes were not provided [5]. Finally, brittle failure mechanism at joint level is observed in recent earthquakes, especially in cases of framed

structures designed for gravity loads only. The accuracy and reliability of theoretical and empirical models available for evaluating shear strength of beam-to-column r.c. joints can be found in [6].

On the other hand, the seismic retrofitting of existing structures, in particular of r.c. framed buildings vulnerable under gravity loads, represents a worrying problem requiring urgent action [2]. To do this, many traditional methods [7], usually adopting conventional materials and construction techniques (e.g. r.c. shear walls, steel braces, steel encasing and concrete jacketing), and modern methods [7–10] based on new techniques and materials (e.g. wrapping by means of carbon fibre reinforced polymers, base-isolation and energy dissipation), can be adopted alone or in combination.

In the present work, a r.c. framed building built sixty years ago with bi-directional (perimeter) and mono-directional (interior) plane frames, originally designed for five storeys then elevated to six during construction, is considered for the numerical investigation. The static vulnerability of the original structure at the ultimate life-safety (LS) limit state is preliminarily investigated. More specifically, alternative chord rotation (at member level) and shear strength (at section and joint levels) capacities are compared, checking the consistency of the results and pointing out the different response of these models. Uncertainties affect each one of these models, as they often adopt simplified analytical

* Corresponding author.
  E-mail addresses: fabio.mazza@unical.it (F. Mazza),
pucci.daniela@outlook.it (D. Pucci).

expressions and do not consider all relevant parameters [11–13]. Then, to improve the static response of the original fixed-base structure (i.e. FB structure), carbon fibre reinforced polymer (CFRP) flexural and shear wrapping of beams and columns is considered (i.e. FB+CFRP structure). Finally, in order to retrofit the FB structure, in a high-risk seismic region, two alternative structural solutions are examined based on a base-isolation system, with elastomeric (i.e. HDLRB) and sliding (i.e. steel-PTFE) bearings, acting alone (i.e. BI structure) or in combination with CFRP (i.e. BI+CFRP structure). To evaluate the effectiveness of the retrofitting strategies, nonlinear analyses are carried out on a three-dimensional fibre model of the original and retrofitted structures [14].

2. Layout and simulated design of the original structure

In the present work, a residential r.c. framed building, built in 1955 and located in Cosenza (Calabria, Italy), is considered (Fig. 1a). It is characterized by bi-directional (perimeter) and mono-directional (interior) plane frames designed to comply with the admissible tension method, in line with the R.D.L. 1939 [15]. It

was designed as a five-storey building but elevated to six-storeys during construction; square and C-shaped plans, with storey heights of 4.25 m and 3.35 m, are considered at the first floor (Fig. 1b) and the other floors (Fig. 1c and d), respectively.

Floor structures are made with cast-in-place mixed r.c. slabs and semi-hollow blocks (i.e. A1 and A2 types) and r.c. solid slabs (i.e. A3 type). The gravity loads are represented by: A1 dead loads of 4.55 kN/m^2, on the top floor, and 5.19 kN/m^2, on the other floors; A2 and A3 dead loads of 5.0 kN/m^2 and 6.66 kN/m^2, respectively, on all floors; A1, A2 and A3 live loads of 2.0 kN/m^2, 0.9 kN/m^2 and 4.0 kN/m^2, respectively. Infill walls are considered regularly distributed in elevation along the perimeter, assuming an average weight of about 2.4 kN/m^2. Although the original design drawings and reports are available, a field survey of the building was performed because the current state highlights differences in terms of in-plan and in-elevation geometry and position and cross-section of frame members. It is worth noting that the deep beams of the perimeter frames are characterized by a narrow cross-section (i.e. b_w=20 cm). Results of pacometric tests done have highlighted diameters of 14 mm–16 mm–18 mm and 12 mm–16 mm for columns and beams, respectively; a low
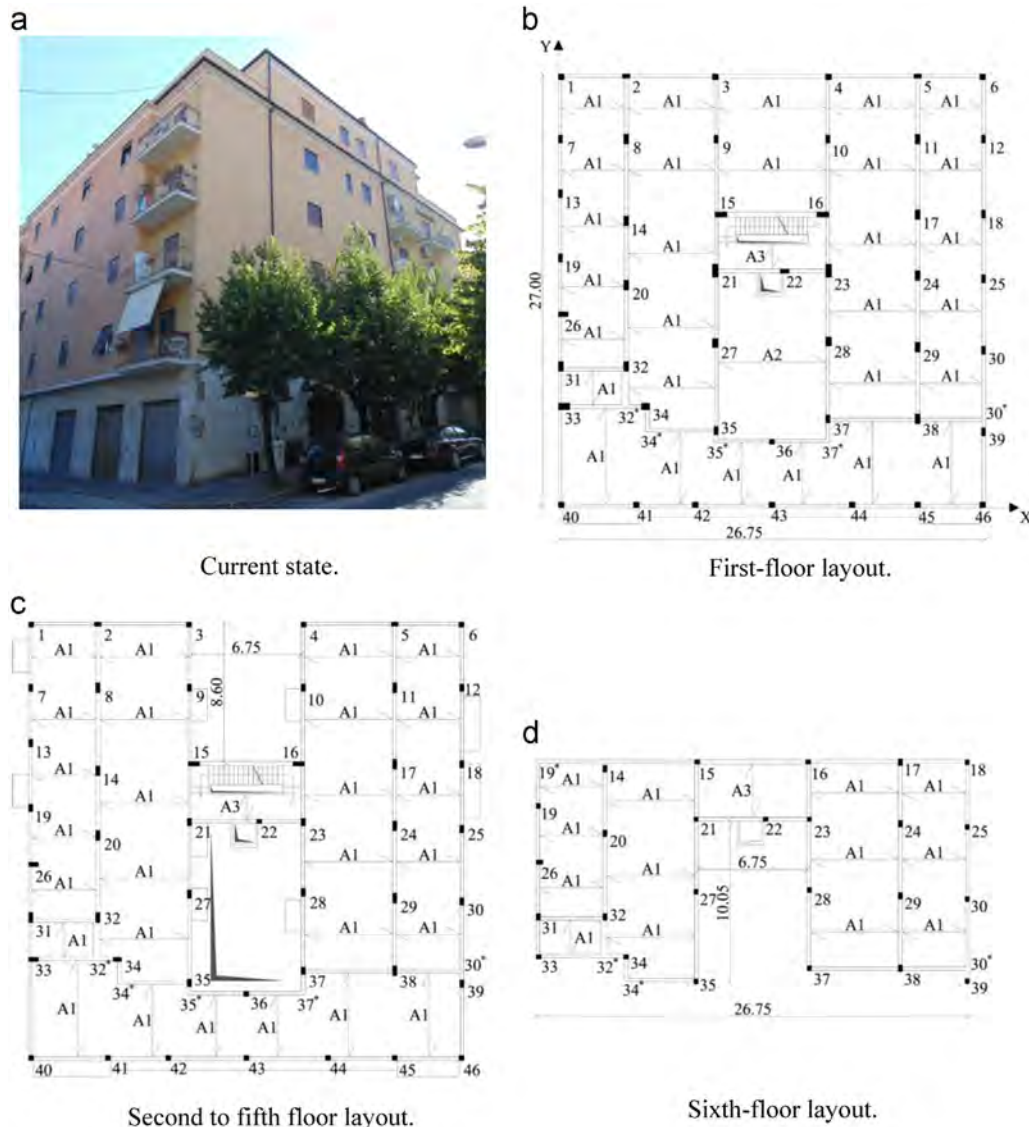
Fig. 1. Test structure (dimensions in m).

a

b

Rebound number versus core testing.

Ultrasonic velocity versus core testing.
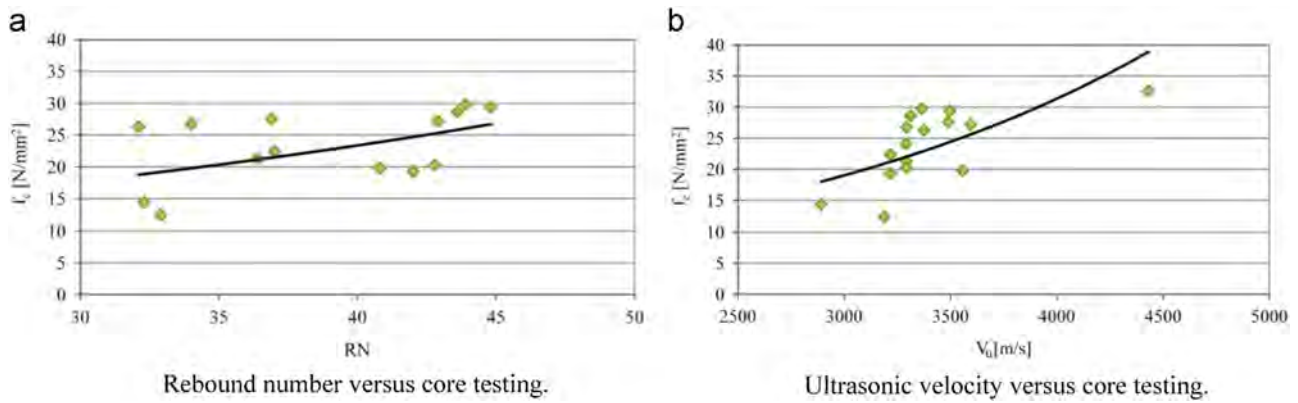
Fig. 2. Correlation between destructive and non destructive results.

Table 1
Dynamic properties of the original structure ($m = 3686\ t$).

Mode	T_i [s]	$m_{E,X}$ [%m]	$m_{E,Y}$ [%m]
1	1.28	59.75	0.03
2	1.10	0.34	80.04
3	1.04	17.92	0.84
4	0.48	8.62	0.00
5	0.43	0.00	11.21
6	0.32	7.29	0.00

Table 2
Mechanical properties of the CFRP sheets.

	E_f [GPa]	f_{fk} [MPa]	ε_{fu} [%]	s [mm]	L [mm]
Dry fibres	230	4800	1.9	0.083	100
Epoxy-bonded fibres	93	382	0.41	0.083	100

(T_i); effective masses in the X ($m_{E,X}$) and Y ($m_{E,Y}$) directions, expressed as percentage of the total mass (m).

confinement level of stirrups in terms of both spacing (18–20 cm) and diameter (6 mm) is found for all members.

Three knowledge levels (KL) and corresponding confidence factor (CF) are defined in Eurocode 8 [16] and NTC08 [17] seismic codes. Specifically, a normal level of knowledge, characterized by CF=1.2, should be obtained by performing limited in-situ testing, when information on the mechanical properties of the construction is available from original design specifications. In the present work, in accordance with KL2, concrete properties are investigated by means of destructive (i.e. core testing) tests and integrated with the results obtained from non-destructive (i.e. sclerometric and ultrasonic) tests. As known, core tests are not representative of the in-structure property variations because only a limited number of them can be carried out in practice. On the other hand, rebound number (RN) and ultrasonic velocity (V_U) methods are quick and inexpensive, but they may provide unreliable predictions of concrete strengths when compared with core tests (Fig. 2). Therefore, a mean value of the concrete cylindrical strength equal to 22.39 MPa is considered in the numerical investigation.

Steel properties are estimated in accordance with both specifications of the original project and test certificates, without removal of longitudinal reinforcement which could compromise the integrity of the structural elements. Moreover, Italian standards in force at the time of construction [15] and types of steel produced and used at that period are also verified; namely, since a Aq50 steel was used, a mean value of yield strength equal to 300 MPa is assumed.

Then, to improve knowledge of the test structure the present work uses a simulated design, with reference to the R.D.L. 1939. The data are enriched with information based on the practical rules and regulations applied at the time of construction [18,19]. Note that some elements of the original structure do not fulfil the verification of the simulated design, with inadequate longitudinal steel reinforcement of beams and cross-section dimension of both columns and beams.

Finally, the dynamic properties of the six main vibration modes, assuming a modulus of elasticity of the concrete equal to $4700 f_c^{0.5}$ MPa [14], are reported in Table 1: i.e. vibration period

3. Retrofit with CFRP wrapping and base-isolation

To improve the structural behaviour of r.c. frame members of the original FB structure it was planned to strengthen these elements by wrapping them with composites. The design of the CFRP was carried out according to the provisions of the new Italian instructions (CNR-DT 200/2013, [20]), considering two cases: i.e. CFRP acting alone (FB+CFRP structure) or in combination with the base-isolation (BI+CFRP structure), to retrofit the original fixed-base structure under gravity and seismic loads, respectively. To this end, CFRP sheets are considered as externally bonded strengthening materials for beams and columns. R.c. beams are strengthened with one layer of CFRP fabric with bidirectional texture, bonded on the tensile side to improve the ultimate positive bending moment, and with one layer transversal U-wraps with bidirectional texture, to improve the shear capacity. R.c. columns are confined continuously with one layer of CFRP fabric with bidirectional texture, to improve both shear capacity and ductility. Table 2 summarizes the following mechanical properties of the dry fibres and fibres mixed with epoxy resin (i.e. epoxy-bonded fibres) considered for the CFRP: Young's modulus (E_f), tensile strength (f_{fk}), ultimate strain (ε_{fu}), thickness (s), width (L).

In Table 3 the results of flexural design for positive moments of the beams B33–34 and B30–39, on the 5th floor, are reported in terms of number ($n_{flex,g}$) and area ($A_{flex,g}$) of the CFRP. The same table also reports the ultimate positive moment with strengthening ($M_{Rd,g}^+$) and its ratio ($\alpha_{flex,g}^+$) with the corresponding value without strengthening with reference to the most stressed section of the selected beams. Results of shear design for the same beams are also shown in Table 4, where the number of U-wraps ($n_{sh,g}$) and their area ($A_{sh,g}$) are reported. Moreover, the shear strength of the strengthened beams ($V_{Rd,g}$) and its ratio ($\alpha_{sh,g}$) with the corresponding value without strengthening, evaluated as the sum of contributions related to concrete and steel stirrups, are shown in Table 4.

Finally, in Table 5 are reported results of the shear design with reference to the columns C26 and C35, on the first storey, C34, on

Table 3
Flexural design of CFRP for beams.

Element	FB+CFRP structure				BI+CFRP structure			
	$n_{flex,g}$	$\alpha_{flex,g}$ [mm^2]	$M_{Rd,g}^{+}$ [kNm]	$\alpha_{flex,g}^{+}$	$n_{flex,g}$	$\alpha_{flex,g}$ [mm^2]	$M_{Rd,g}^{+}$ [kNm]	$\alpha_{flex,g}^{+}$
B33-34, 5th floor	2	33.2	104	2.21	2	33.2	104	2.21
B30-39, 5th floor	3	49.8	91	2.27	3	49.8	91	2.27

Table 4
Shear design of CFRP for beams.

Element	FB+CFRP structure				BI+CFRP structure			
	$n_{sh,g}$	$A_{sh,g}$ [mm^2]	$V_{Rd,g}$ [kN]	$\alpha_{sh,g}$	$n_{sh,g}$	$A_{sh,g}$ [mm^2]	$V_{Rd,g}$ [kN]	$\alpha_{sh,g}$
B33-34, 5th floor	2	33.2	153	1.38	3	49.8	174	1.55
B30-39, 5th floor	2	33.2	128	1.36	3	49.8	145	1.52

Table 5
Shear design of CFRP for columns.

Element	FB+CFRP structure				BI+CFRP structure			
	$n_{sh,c}$	$A_{sh,c}$ [mm^2]	$V_{Rd,c}$ [kN]	$\alpha_{sh,c}$	$n_{sh,c}$	$A_{sh,c}$ [mm^2]	$V_{Rd,c}$ [kN]	$\alpha_{sh,c}$
C26, 1st storey	–	–	–	–	3	49.8	98	1.58
C34, 2nd storey	–	–	–	–	1	16.6	85	1.31
C35, 1st storey	–	–	–	–	1	16.6	85	1.44
C33, 4th storey	2	33.2	58	1.56	2	33.2	58	1.56

Table 6
Flexural verification for the floor slabs.

s [cm]	h_r [cm]	b_r [cm]	i_r [cm]	M_d^{+} [kNm]	M_d^{-} [kNm]	α^{+}	α^{-}
4	18	12	62	11.8	14	0.97	0.99

the second storey, and C33, on the fourth storey. In detail, the following parameters are presented: number ($n_{sh,c}$) and area ($A_{sh,col}$) of the CFRP sheets; shear strength of the strengthened columns ($V_{Rd,c}$) and its ratio ($\alpha_{sh,c}$) with corresponding value without strengthening.

At all levels of the original structure, floor slabs do not require strengthening with CFRP. More specifically, Table 6 illustrates the results of the flexural verification, in terms of positive (M_d^{+}) and negative (M_d^{-}) design moments and their ratio with the corresponding flexural strengths (i.e. α^{+} and α^{-}). The following geometric dimensions are reported: thickness of slab (s); height (h_r), width (b_r) and centre distance (i_r) of the ribs. Further results, omitted for brevity, confirm that the shear verification is also satisfied.

For the purpose of retrofitting the original FB structure, given high-risk seismic region and a medium subsoil class (i.e. class B, site amplification factor S=1.136), an in-parallel combination of elastomeric (i.e. high-damping-laminated-rubber bearings, HDLRBs) and friction (i.e. steel-PTFE sliding bearings, SBs) isolators was considered (i.e. BI structure). Afterwards, local strengthening of the base-isolated structure was carried out by wrapping beams and columns with composite materials (i.e. carbon fibre reinforced polymer, CFRP), to improve their flexural and shear capacities (i.e. BI+CFRP structure). In the design of the base-isolated structure a fundamental vibration period T_{IH}=4.0 s and equivalent viscous damping ratio ξ_{IH}=15% are assumed in the horizontal direction. The proportioning of the base-isolation system was carried out on the assumption that, besides the gravity loads, the horizontal loads correspond to a behaviour factor q=1.0; the acceleration design spectrum is modified in the period range $T \geq 0.8T_{IH}$, with $T_{IH} \geq 3T_{BF}$, T_{BF}=1.28 s being the fundamental vibration period of the same structure on fixed-base. As shown in Fig. 3, the BI retrofitted structure is supported by 22 HDLRBs and 24 steel-PTFE SBs.

More specifically, perimeter and interior HDLRBs are assumed with the same dimensions in the building plan, for the sake of simplicity and in order to obtain a larger torsional stiffness. The design of the in-parallel combination of HDLRBs and steel-PTFE SBs is carried out in order to increase the secondary shape factor of the elastomeric bearings in comparison with the solution adopting only HDLRBs. To this end, a value equal to 0.534 is assumed for the nominal sliding ratio $\alpha_{S0}(=F_{S0}/F_{S0,max})$ of the SBs under gravity loads, defined as the global sliding force (F_{S0}) divided by the maximum sliding force ($F_{S0,max}$); this latter one evaluated supposing that sliding bearings are placed under each column. Finally, the in-plan arrangement of HDLRBs and SBs is assumed in order to
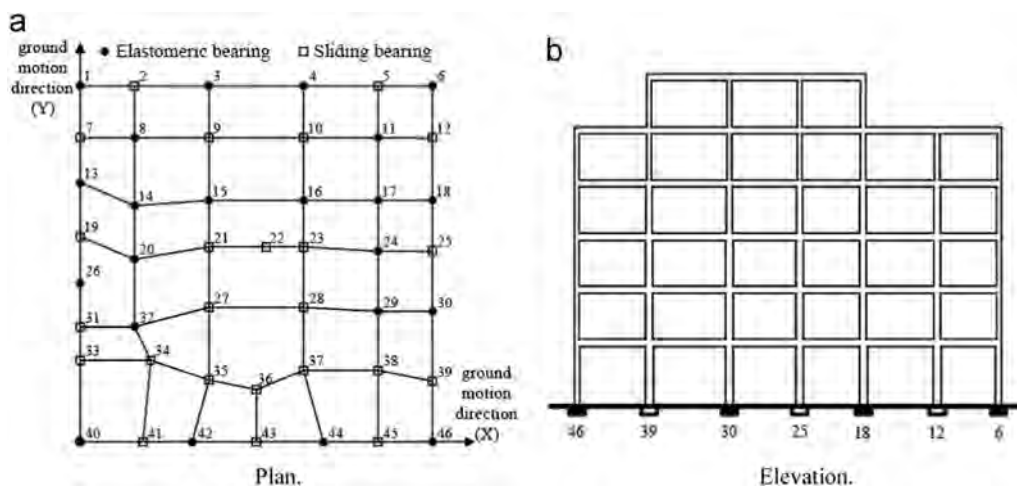
Fig. 3. Base-isolated retrofitted structure (m_{tot}= 4386 t).

Table 7
Geometric properties of the HDLRBs.

D [mm]	t_i [mm]	n_i	t_s [mm]	d_{dC} [mm]
645	8	33	2	290

Table 8
Results of the verifications for the HDLRBs.

S_1	S_2	γ_s	$\gamma_{tot,max}$	V_{cr}/V_{max}	V_{cr} [kN]
19.97	2.43	1.10	3.05	2	2760

limit, at the foundation level, the eccentricity between the stiffness centre of the base-isolation system and the projection of the centre of mass of the superstructure.

In detail, the HDLRBs fulfil the ultimate limit state verifications regarding the maximum shear strains: i.e. $\gamma_{tot} = \gamma_s + \gamma_c + \gamma_\alpha \le 5$ and $\gamma_s \le 2$, where γ_{tot} represents the total design shear strain, while γ_s, γ_c and γ_α represent the shear strains of the elastomer due to seismic displacement, axial compression and angular rotation, respectively. Moreover, the maximum compression axial load (P) did not exceed the critical load divided by a safety coefficient equal to 2.0. The critical buckling load was evaluated as a function of the original S_1 (e.g. $S_1 \ge 12$ is a conservative assumption to reduce the vertical deformability) and secondary S_2 (e.g. $S_2 \ge 4$ is a conservative assumption against buckling) shape factors [21]. The minimum tensile stress (σ_t) resulting from the seismic analysis was assumed as $2G(=0.8$ MPa, for a shear modulus of the elastomer $G=0.4$ MPa). Finally, the volumetric compression modulus of the rubber (i.e. E_b) is assumed equal to 2000 MPa. Table 7 reports the following geometric and mechanical properties: diameter of the bearing (D); thickness of a single elastomeric layer (t_i); number of elastomeric layers (n_i); thickness of a single steel shim (t_s), with a yield strength of 255 MPa; displacement at the collapse prevention limit state (d_{dC}).

Table 8 displays the results of the ultimate collapse prevention limit state verifications for the HDLRBs. It is worth noting that the design of the isolators depends on the conditions imposed on the maximum values of γ_{tot} and γ_s and the buckling control; no tensile forces were found in the isolators.

4. Capacity models of r.c. frame members and joints

To evaluate the vulnerability of frame members and joints of the original structure, the capacity models provided by the Italian (NTC08, [18]) and European (Eurocode 8, [17]) seismic codes and other guidelines (CNR-DT 212/2013, [22]) and expressions [6] available in the scientific literature are considered. Most of these formulae are calibrated in line with experimental results, thus requiring practical application for vulnerability assessment of existing structures to evaluate their effectiveness. At the ultimate life-safety (LS) limit state, ductile modes of r.c. frame members will be checked in terms of chord rotation while the brittle ones will be assessed in terms of shear strength at section level, both referring to the expressions proposed by the above mentioned codes and guideline. The aim of this first choice is to check the consistency of the results obtained applying the three codes proposed. Moreover, many analytical models are currently available for evaluating the shear capacity of beam-to-column joints in r.c. framed structures. Main objective of the second choice is to verify the reliability of the simplified approaches adopted by the Italian and European codes.

Ductile modes of the original structure are checked through the evaluation of the chord rotation at the end sections of each r.c.

frame member. Chord rotation capacity depends both on the geometric and mechanical properties of the frame member and on the gravity and seismic loads. The expression of the member chord rotation provided by NTC08 [18] and EC8 [17] is compared with the ones proposed by Zhu [23] and Haselton [24] and reported in the CNR-DT 212 guidelines [22]. In detail, the ductile mechanism is reached at the member level when the maximum value of the chord-rotation demand (θ_{max}) is equal to the corresponding ultimate value. To take into account the bi-directionality of chord rotations, the following threshold curve is considered for columns

$$\left(\overline{\theta}^{(X)}\right)^2 + \left(\overline{\theta}^{(Y)}\right)^2 = 1 \, , \overline{\theta}^{(q)} = \theta_{max}^{(q)}/\theta_u^{(q)}, q \in (X, \, Y) \tag{1}$$

Brittle modes of the original structure are assessed at the section level through the evaluation of the shear capacity at the end sections of each r.c. frame member. The expressions proposed by NTC08 and EC8 are compared with that proposed by Sezen and Moehle [25] and recommended in the CNR-DT 212 guidelines [22]. A check for the brittle mechanisms is performed at section level, through the evaluation of the maximum shear demand (V_{max}) and the corresponding capacity at the two ends of each structural member:

$$\left(\overline{V}^{(X)}\right)^2 + \left(\overline{V}^{(Y)}\right)^2 = 1 \, , \overline{V}^{(q)} = V_{max}^{(q)}/V_u^{(q)}, q \in (X, \, Y) \tag{2}$$

It is worth noting that dimensionless chord rotation ($\overline{\theta}$) and shear force ($\overline{V}$) along the major axis of the cross section are considered for the beams.

Finally, brittle modes of the r.c. joints are evaluated adopting the capacity models proposed by NTC08, EC8 and empirical expressions proposed by Hegger [26] and Kim [27]. To this end, the damage observed in the r.c. beam-to-column joints was investigated considering the shear strength (V) and the principal stresses of the concrete (σ). To this end, dimensionless nodal resistances

$$\overline{J}_V = V_{max}/V_u \, , \quad \overline{J}_\sigma = \sigma_{max}/\sigma_u \tag{3}$$

are evaluated in the perimeter, corner and interior joints.

5. Numerical results

In order to study the nonlinear behaviour of the original and retrofitted structures above described, three-dimensional fibre models are considered [14]. Force-based fibre elements for beams and columns and special elements for CFRP-wrapping of the frame members (Fig. 4a) and elastomeric (i.e. HDLRBs) and friction (i.e. SBs) isolators (Fig. 4b) are considered in the SeismoStruct computer program. In detail, each frame member is modeled with a force-based element, considering five integration sections to capture the inelastic behaviour along the entire length. Square and rectangular cross-sections are subdivided into 100 fibres. The low confinement level of stirrups is not incorporated in the concrete model [28], while the cyclic behaviour of concrete is described [29]; moreover, the reinforcing longitudinal steel is modeled with a bilinear law. In the nonlinear dynamic analysis the integration of the equations of motion is accomplished using the implicit iteration algorithm proposed by Newmark, with a time step $\Delta t = 0.01$ s and an automatic time-step adjustment for optimum accuracy and efficiency [14]. Moreover, P-delta effects are also taken account.

Viscoelastic (linear) force-displacement laws idealize the behaviour of the HDLRBs (Fig. 4c), in the horizontal (F-u_H) and vertical (P-u_V) directions, while a rigid-plastic law, with a friction threshold F_f equal to a friction coefficient (μ) multiplied by the vertical load (P), is considered for the steel-PTFE sliding bearings (Fig. 4d). An elastic linear law idealizes the behaviour of the CFRP up to tension failure, without post-peak response and resistance in

a

Fixed-base original structure.

b

Base-isolated retrofitted structure.

c

$F(P)$

$K_H(K_V)$

$u_H(u_V)$

HDLRB force-displacement law.

d

F

$F_f = \mu P$

u_H

$-F_f$

SB force-displacement law.

e

σ_f

f_{fk}

E_f

ε_{fu}

ε_f

CFRP constitutive law.
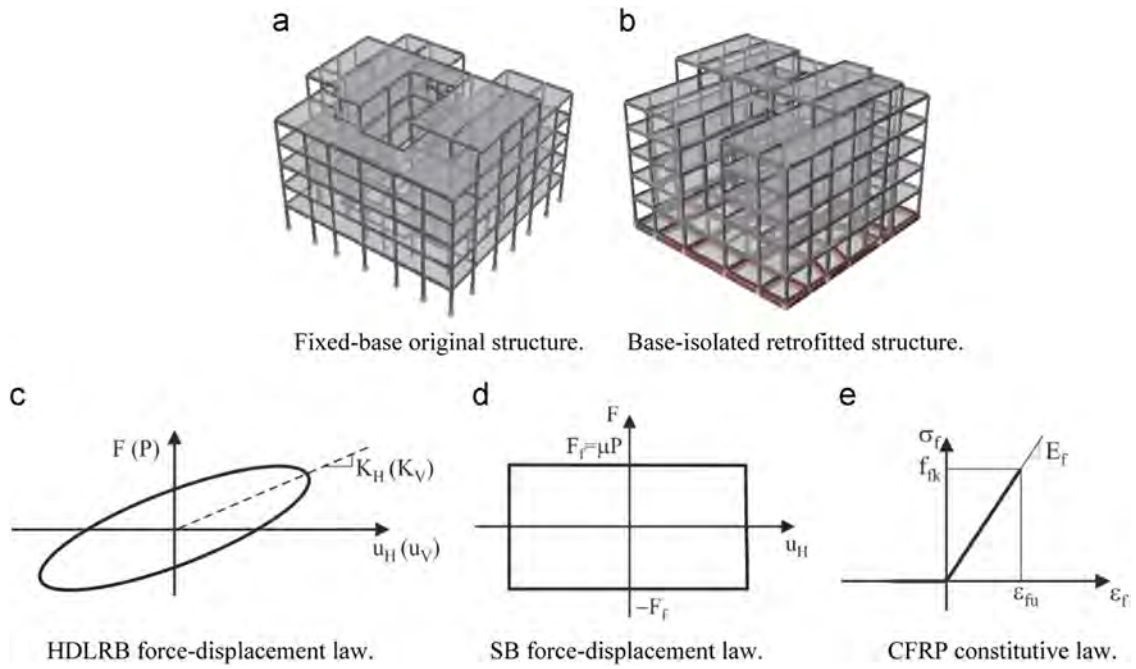
Fig. 4. Modeling of the test structure.

a

□EC8-NTC08 ▨ZHU ▦HASELTON

C 41

C 40

C 34

C 16

$\left(\bar{\theta}^{(x)}\right)^2 + \left(\bar{\theta}^{(y)}\right)^2$

Columns at 1st storey.

b

□EC8-NTC08 ▨ZHU ▦HASELTON

C 37

C 40

C 34

C 16

$\left(\bar{\theta}^{(x)}\right)^2 + \left(\bar{\theta}^{(y)}\right)^2$

Columns at 3rd storey.

c

□EC8-NTC08 ▨ZHU ▦HASELTON

B 15-16

B 32-32*

B 8-14

B 21-22

B 31-33

B 40-41

$\bar{\theta}$

Beams at 5th floor.
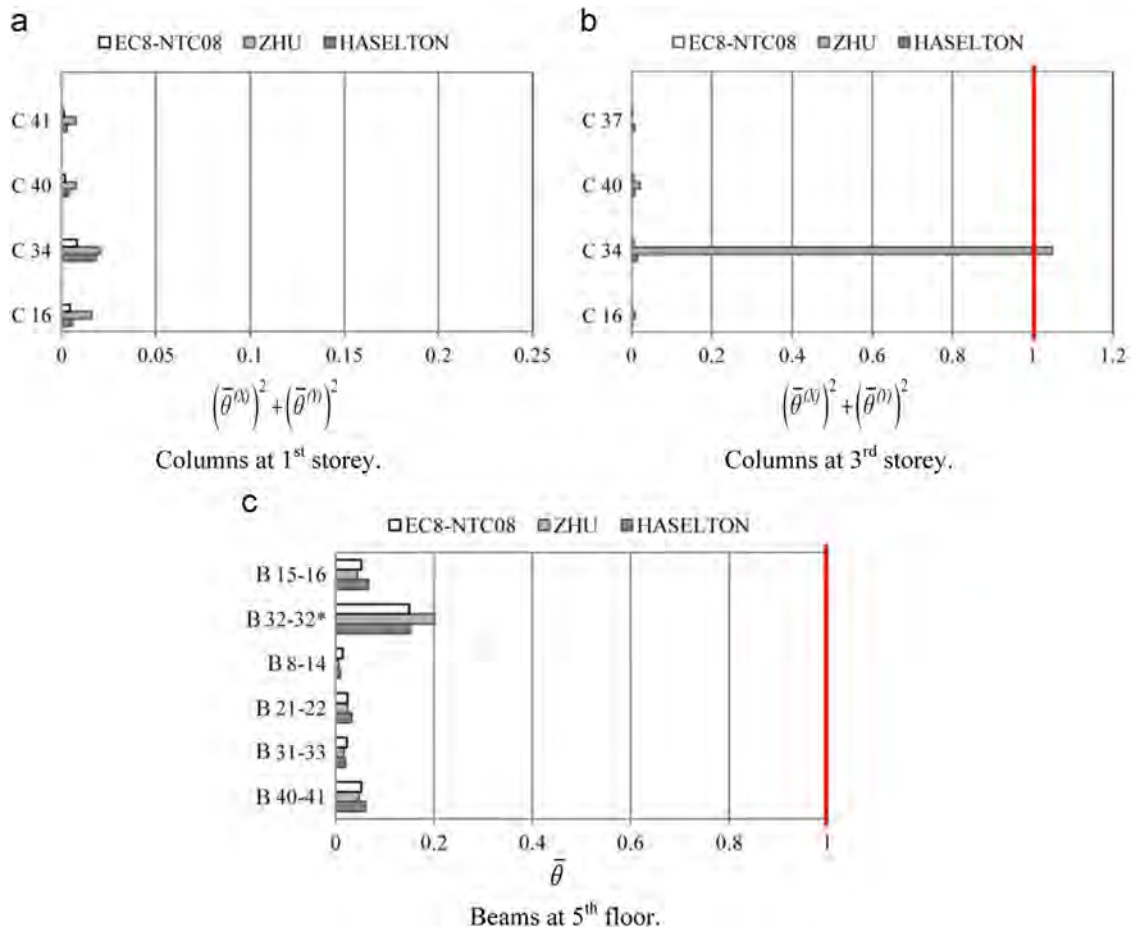
Fig. 5. Dimensionless chord rotation for the FB structure under static loads.

compression. (Fig. 4e). The rigid in-plane stiffness of the floor slab is modelled as a rigid diaphragm with elastic truss elements. Finally, masonry infills are considered as nonstructural elements and their contribution is neglected in the nonlinear analysis of the retrofitted structures.

First, a numerical investigation is carried out to study the vulnerability of the original structure under gravity loads. The flexural response of the test structure was examined in Fig. 5, with reference to columns, at first (Fig. 5a) and third (Fig. 5b) storeys, and beams, at fifth floor (Fig. 5c).

More specifically, in line with the Italian and European (EC8-NTC08), Zhu and Haselton models, the dimensionless chord rotation was evaluated for the most stressed structural elements: i.e. lateral (C41 and C37), corner (C40), central (C34) and stair (C16) columns shown in Fig. 1b and c; perimeter and interior deep beams, along the in-plan X (B40-41 and B21-22) and Y (B31-33 and B8-14) directions, and flat (B32-32*) and stair (B15-16) beams shown in Fig. 1c. The chord rotation dimensionless threshold was also plotted with a red line in Fig. 5b and c. As can be observed, almost all frame members satisfy the LS limit state and a "strong column-weak beam" mechanism is obtained due to the greater values of $\bar{\theta}$ for the beams. In the case of the columns, the EC8-NTC08 and Zhu models provide, respectively, the lowest and highest values of dimensionless chord rotation. Moreover, unrealistically negative or small values of ultimate chord rotation are obtained adopting the Zhu model for the columns, when high values of the ratio between the spacing of the stirrups and the section depth and the normalized axial load are considered. This happens for the columns C37, whose dimensionless chord rotation

is not reported, and C34, both at third storey (Fig. 5b). On the other hand, only slight differences of $\bar{\theta}$ are generally obtained when different models for the beams are assumed (Fig. 5c). As expected, the B32-32* flat beam is resulted more deformable than deep beams shown in Fig. 5c.

Analogous results are reported in Fig. 6, with reference to the maximum shear force in the columns, at second (Fig. 6a) and fourth (Fig. 6b) storeys, and beams, at fifth floor (Fig. 6c). In this case, the EC8, NTC08 and Sezen and Moehle models are compared, considering: lateral (C33 and C35), corner (C40), central (C34) and stair (C15 and C16) columns shown in Fig. 1b and c; perimeter and interior deep beams, along the in-plan X (B40-41 and B33-34) and Y (B30-39 and B8-14) directions, and flat (B32-32*) and stair (B15-16) beams shown in Fig. 1c.

Also in this case, maximum shear forces less than the corresponding ultimate values were achieved for almost all the columns, but a wide variation of the dimensionless shear force is found when using different models (e.g. see columns C35 and C33 in Fig. 6a and b, respectively). Beams exceeded their shear thresholds, especially when the EC8 model was adopted, while comparable values of $\bar{V}$ were obtained when the NTC08 and Sezen and Moehle models were considered (Fig. 6c). Generally, EC8 model resulted more conservative than the other models. Moreover, for all capacity models, lateral and central columns shown in Fig. 6a and b are characterized by higher values of dimensionless shear force than those observed in the corner and stair columns; similar result is also obtained for the B33-34 and B30-39 beams, with a narrow cross-section, in comparison with the other beams reported in Fig. 6c.
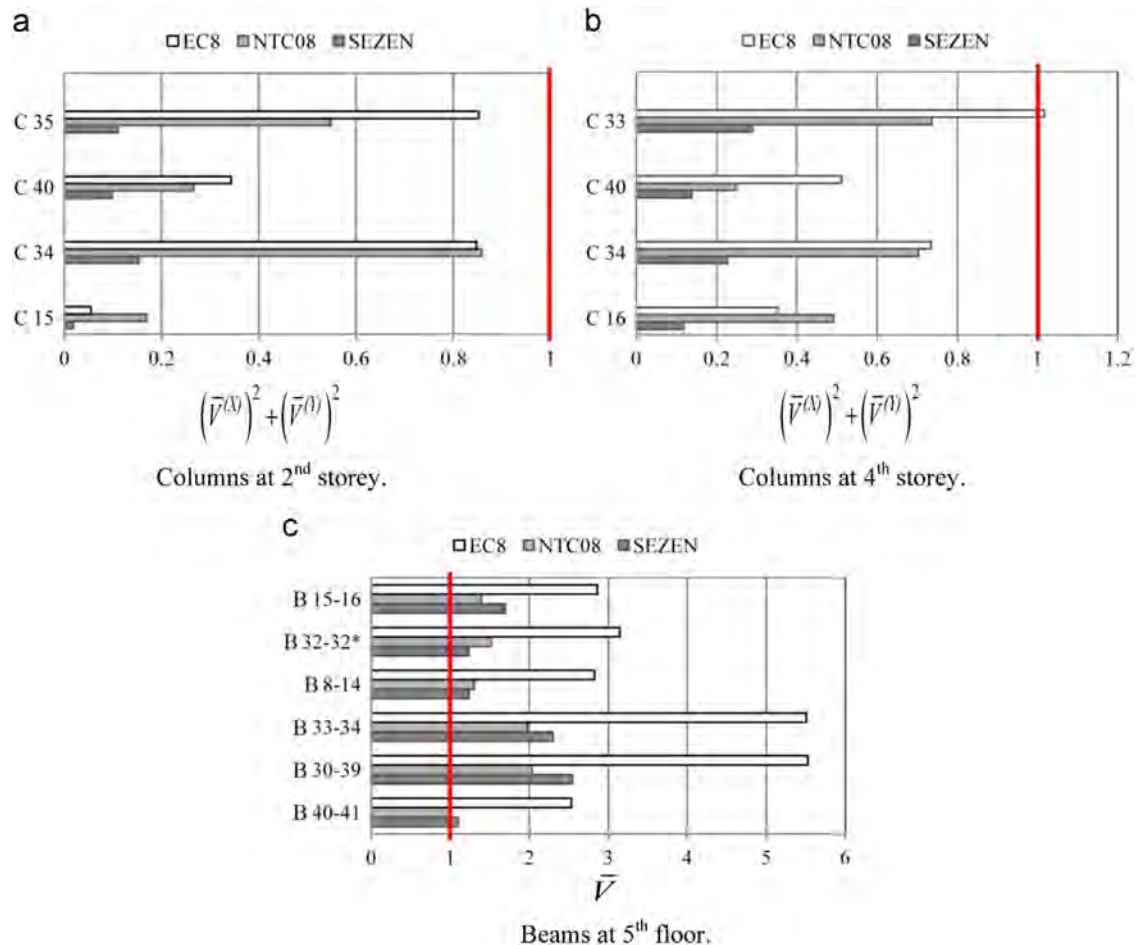
Fig. 6. Dimensionless shear force for the FB structure under static loads.
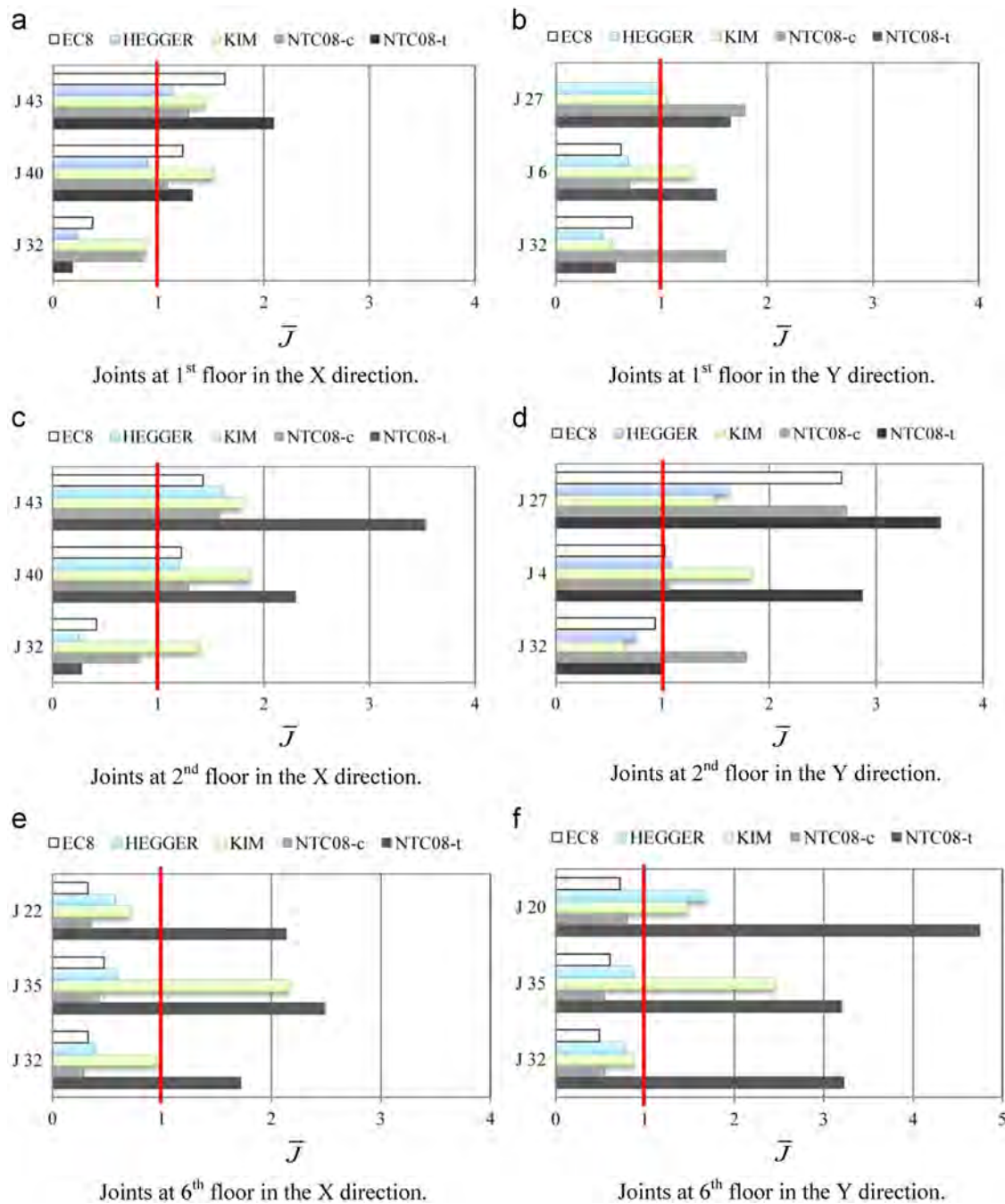
Fig. 7. Dimensionless nodal resistance for the FB structure under static loads.

Next, the damage observed in the r.c. beam-to-column joints was investigated in Fig. 7, considering the shear strength (V) in the EC8, Hegger and Kim models and the principal stresses of the concrete (σ), in tension (NTC08-t) and compression (NTC08-c).

To this end, dimensionless nodal resistances in the perimeter (J22, J27 and J43), corner (J4, J6, J35 and J40) and interior (J20 and J32) unreinforced joints were plotted along the in-plan X (Fig. 7a, c, and e) and Y (Fig. 7b, d, and f) directions. As expected, the results scattered considerably for the different expressions, because of the numerous set of geometric and mechanical parameters influencing the structural response of r.c. joints, which are often calibrated on a rather limited number of experimental results. It is worth noting that the EC8 model fails in some cases: e.g. see joint J27 in Fig. 7b, whose EC8 value is not reported; moreover, NTC08-c and NTC-t

models are often too conservative in comparison with the other models.

The percentage of columns and beams satisfying the EC8 shear threshold along the building height is reported in Fig. 8a. It is worth noting that almost 100% of the columns are found to verify the shear threshold, contrary to 10% of the beams for the first five floors. The percentage of joints satisfying the EC8 shear threshold at the floor levels is reported in Fig. 8b, which distinguishes the in-plan X and Y directions. Note that the joints are more vulnerable along the Y direction, with the only exception being on the third floor. Further results, omitted for the sake of brevity, confirm a percentage of beams and columns verified to the EC8 flexural threshold equal to 100%.

Then, the static behaviour of the fixed-base CFRP-retrofitted (i.e. FB+CFRP) structure is examined under gravity loads, checking

Elements verified to EC8 threshold.   Joints verified to EC8 threshold.
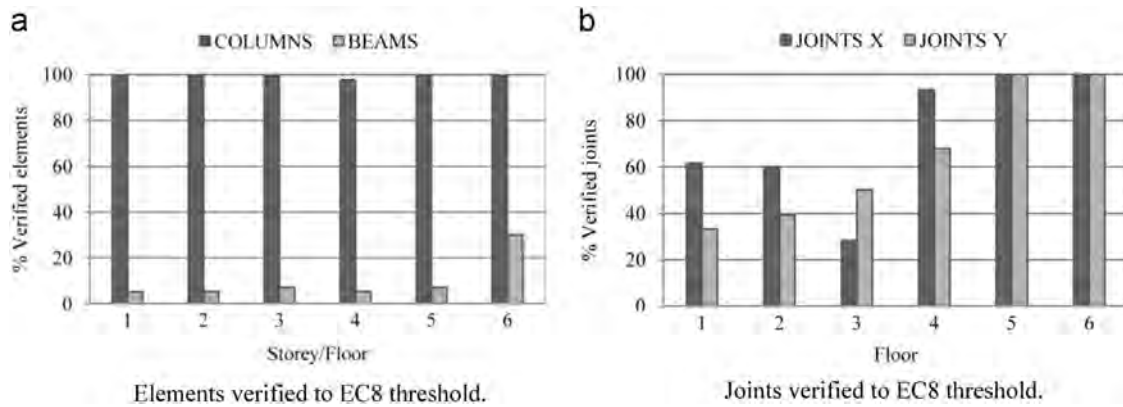
Fig. 8. Percentage of elements and joints satisfying the EC8 shear threshold for the FB structure.

Dimensionless shear force.   Beams verified to EC8 threshold.
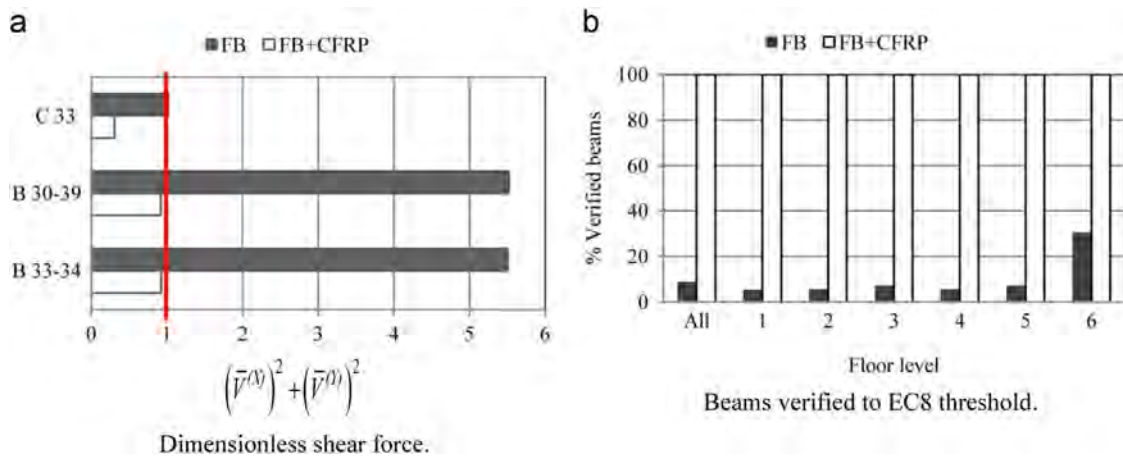
Fig. 9. Shear verification of the beams for the FB and FB+CFRP structures under static loads.

the shear threshold imposed by EC8. To this end, maximum values of the dimensionless shear force are plotted in Fig. 9a, with reference to the most stressed column (i.e. C33 at fourth storey) and beams (i.e. B30-39 and B33-34 at fifth floor) highlighted in Fig. 6b and c, respectively.

Note that an effective increase in ultimate shear force, with a dimensionless value less than 1, is obtained for the FB+CFRP retrofitted structure in comparison with the original (i.e. FB) structure. Moreover, the percentage of beams satisfying the EC8 shear threshold along the building height is reported in Fig. 9b. As shown, the total amount of these elements verifies the shear threshold at all floor levels in the FB+CFRP structure, contrary to a small percentage in the case of the FB structure. For the purpose of retrofitting the original structure to attain the performance levels imposed by NTC08 in a high-risk seismic zone, innovative technology, such as base-isolation with HDLRBs and SBs, and innovative materials, such as CFRP, are adopted in the present work.

To evaluate the effects of the proposed retrofitting technique on the seismic response of the original structure, nonlinear dynamic analysis is carried out considering two horizontal accelerograms applied simultaneously along the X and Y principal directions of the building plan (see Fig. 3a). In accordance with the minimum number of artificial motions imposed by EC8 [16] and NTC08 [17], three pairs of accelerograms, each with a duration of the stationary part equal to 10 s and a total duration of 25 s, are generated using the computer code SIMQKE [30]. In Fig. 10a and b the acceleration (elastic) response spectra of these motions are compared with that adopted by NTC08 for the life-safety (LS) limit state, assuming an elastic viscous damping $\xi=15\%$. As shown, the response spectra of the simulated accelerograms match NTC08

spectrum in the range of vibration periods 0.05–5 s, which also contains the lower and upper limits of the vibration period prescribed by NTC08 for base-isolated structures (i.e. $T_{min}=0.2T_{I,H}$ and $T_{max}=1.2T_{I,H}$, where $T_{I,H}$ is the fundamental vibration period of the isolated structure).

In Table 9, taking into account the assumptions made with regard to seismic intensity (i.e. high-risk) and medium subsoil class (i.e. class B), the following main data are also reported at the LS limit state provided by NTC08: peak ground acceleration on rock, a_g; maximum spectrum amplification coefficient, F_0; vibration period that marks the start of the constant velocity branch of the design spectrum, T_C^*; site amplification factor, $S=S_S \cdot S_T$. It is worth noting that the bi-directionality of the horizontal seismic loads induces bi-directional chord rotation and shear force in the columns, while the effects of in-plan irregularity of the structural configuration are limited in the BI and BI+CFRP structures due to the effectiveness of the base-isolation system to reduce torsional rotations of the superstructure. All the following results are obtained as an average of those obtained separately for each pair of artificial motions.

Dimensionless shear force of the base-isolated retrofitted structures without (i.e. BI) and with (i.e. BI+CFRP) local strengthening of the frame members is plotted in Fig. 11, to check local damage in the columns of the first (C26 and C35), second (C34) and fourth (C33) storeys (Fig. 11a) and beams of the fifth floor level (Fig. 11b). It is interesting to note that the BI retrofitted structure proves unable to avoid EC8 brittle failure of the frame members, while an overall increase in shear force resistance is obtained in the case of the BI+CFRP retrofitted structure. It should be noted that CFRP wrapping is activated only for the horizontal seismic loads,

also considering the gravity loads of the foundation level above the isolation system. Further results, omitted for the sake of brevity, confirm that the BI+CFRP structure satisfies flexural failure modes imposed by EC8, while the BF+CFRP structure is found to be ineffective in controlling the EC8 shear force threshold in beams and columns, due to seismic loads higher than in the BI+CFRP structure.

As in confirmation, the percentage of elements satisfying the EC8 shear threshold along the building height is reported in Fig. 12 for the BI and BI+CFRP retrofitted structures, distinguishing between columns (Fig. 12a) and beams (Fig. 12b). It is worth noting that almost 100% of columns are found to verify the shear threshold in the BI structure, unlike a small percentage of beams, less than 10%. The retrofitted BI structure therefore requires a combination with CFRP local strengthening to control the shear threshold of the beams (Fig. 12b).

6. Conclusions

The investigation focuses on critical aspects in the evaluation of the static vulnerability and seismic retrofitting of a residential six-storey r.c. framed building built in 1955. The present work starts surveying the structure and its materials and a simulated design with reference to the codes in force at the time of construction.

A nonlinear static analysis under gravity loads is carried out considering a three-dimensional fibre model of the original structure, to investigate ductile, at member level, and brittle, at section and joint level, mechanisms. The following conclusions can be drawn from the results.

– The percentage of structural elements verifying the dimensionless chord rotation is equal to 100%, with reference to EC8-NTC08 and Haselton models, while an unrealistically negative value of the ultimate chord rotation can be obtained for the columns adopting the Zhu model. On the other hand, only slight differences of $\bar{\theta}$ are generally obtained when different models for the beams are considered.
– Shear forces less than the corresponding ultimate values are achieved for almost all columns, but a large variability of the dimensionless shear force is found to be when EC8, NTC08 and Sezen models are used. Moreover, beams exceed their shear thresholds, especially when the EC8 model is adopted, while comparable values are obtained for the NTC08 and Sezen models. It is worth noting that almost 100% of the columns are found to verify the EC8 shear threshold, contrary to 10% of the beams for the first five floors.
– A large scatter in the nodal resistance of perimeter, corner and interior unreinforced joints is obtained for the EC8, NTC08,
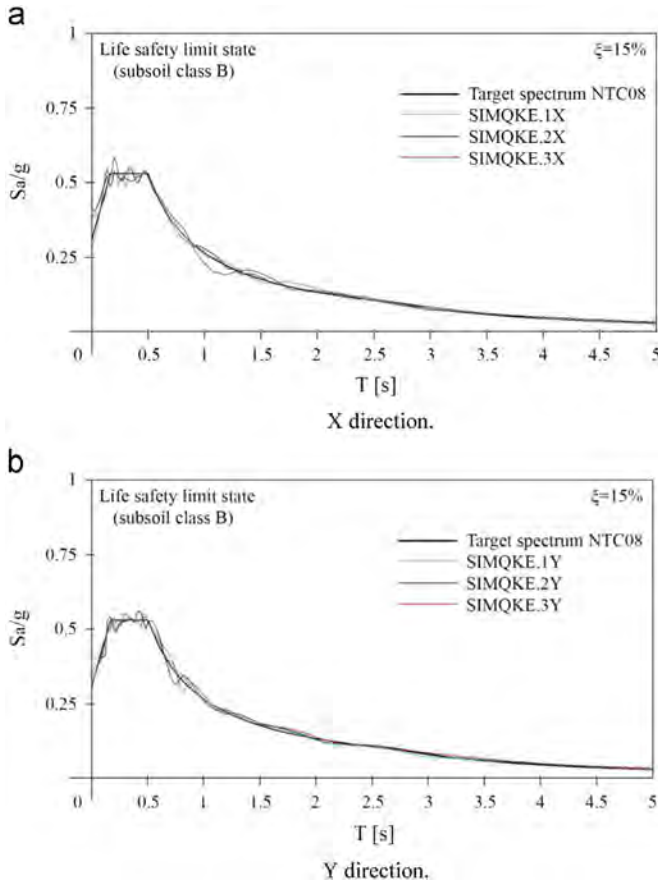
Fig. 10. Acceleration (elastic) response spectra of artificially generated ground motions.

Table 9
Main data to evaluate the horizontal seismic loads.

a_g (g)	F_0	T_C^* [s]	S
0.271	2.432	0.372	1.136
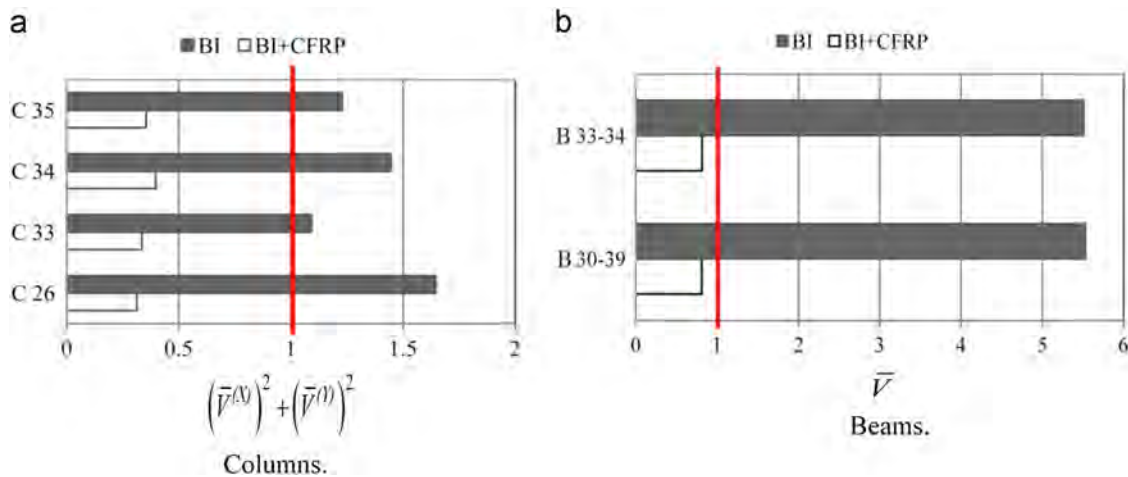
Fig. 11. Maximum dimensionless shear force for the BI and BI+CFRP structures under seismic loads.
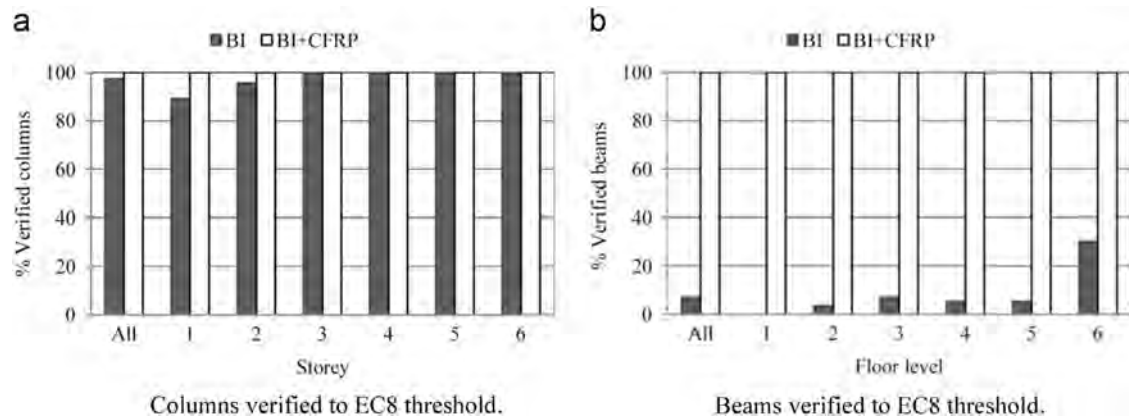
Fig. 12. Percentage of elements satisfying the EC8 shear threshold for the BI and BI+CFRP structures under seismic loads.

Hegger and Kim models, because of the numerous set of geometric and mechanical parameters influencing the structural response of r.c. joints, which are often calibrated on a rather limited number of experimental results. It is worth noting that the EC8 model fails in some cases, while NTC08-c and NTC-t models are often too conservative. At first four levels the joints are more vulnerable along the Y direction, with the only exception being on the third floor.

Vulnerability of the original structure under gravity loads can be removed with local CFRP external strengthening of columns and beams. More specifically, an effective increase in ultimate shear force, with a dimensionless value less than 1, is obtained for the FB+CFRP structure in comparison with the FB structure.

Then, for the purpose of retrofitting the test structure in a high-risk seismic zone, two retrofitting solutions are considered from the original structure, by incorporating base-isolation either alone or in combination with CFRP (i.e. BI and BI+CFRP structures). Even though more case studies are still needed to validate the overall results, the following conclusions can be drawn from the comparison of the nonlinear dynamic biaxial responses. The BI structure is satisfactory as regards the flexural failure modes imposed by EC8 but it proves to be unable to avoid EC8 shear failure of the beams. Almost all columns are found to verify the shear threshold in the BI structure, but only a small percentage of the beams, less than 10%. As expected, the BF+CFRP structure is ineffective in controlling the EC8 shear force threshold in beams and columns, due to seismic loads higher than in the BI+CFRP structure. On the other hand, an overall increase in shear force resistance is obtained in the case of the BI+CFRP structure. As shown above, the BI and BF+CFRP structures are ineffective in controlling certain limit states and thus the BI+CFRP structure is required.

Acknowledgement

References

[1] Masi A, Vona M. Experimental and numerical evaluation of the fundamental period of undamaged and damaged rc buildings. Bull Earthq Eng 2010;8:643–56.

[2] Verderame GM, Polese M, Cosenza E. Vulnerability of existing R.C. buildings under gravity loads: a simplified approach for non sway structures. Eng Struct 2009;31:2141–51.

[3] Mazza F. Comparative study of the seismic response of RC framed buildings retrofitted using modern techniques. Earthq Struct 2015;9(1):29–48.

[4] Verderame GM, Ricci P, Manfredi G, Cosenza E. Ultimate chord rotation of RC columns with smooth bars: some considerations about EC8 prescriptions. Bull Earthq Eng 2010;8(6):1351–73.

[5] De Luca F, Verderame GM. A practice-oriented approach for the assessment of brittle failures in existing reinforced concrete elements. Eng Struct 2013;48:373–88.

[6] Lima C, Martinelli E, Faella C. Capacity models for shear strength of exterior joints in RC frames: state-of-the-art and synoptic examination. Bull Earthq Eng 2012;10:967–83.

[7] Calvi GM. Choices and criteria for seismic strengthening. J Earthq Eng 2013; 17(6):769–802.

[8] Tirca LD, Foti D, Diaferio M. Response of middle-rise steel frames with and without passive dampers to near-field ground motions. Eng Struct 2003; 25(2):69–179.

[9] Sorace S, Terenzi G. Seismic protection of frame structures by fluid viscous damped braces. J Struct Eng 2008;134:45–55 ASCE.

[10] Baratta A, Corbi I, Corbi O, Barros RC, Bairrão R. Shaking table experimental researches aimed at the protection of structures subject to dynamic loading. Open Constr Build Technol J 2012;6:355–60.

[11] Mpampatsikos V, Nascimbene R, Petrini L. A critical review of the R.C. frame existing building assessment procedure according to Eurocode 8 and Italian seismic code. J Earthq Eng 2008;12(S1):52–82.

[12] Romão X, Delgado R, Costa A. Practical aspects of demand and capacity evaluation of RC members in the context of EC8-3. Earthq Eng Struct Dyn 2010;39:473–99.

[13] Mazza F. Modeling and nonlinear static analysis of reinforced concrete framed buildings irregular in plan. Eng Struct 2014;80:98–108.

[14] SeismoStruct. A computer program for static and dynamic nonlinear analysis of framed structures; 2010. Available from URL: ⟨http://www.seismosoft.com⟩.

[15] Royal Decree-Law Regulations for the construction of not reinforced and reinforced buildings (in Italian); 1939. n.2229.

[16] Eurocode 8 Design of Structures for Earthquake Resistance – Part 3: Assessment and retrofitting of buildings; 2004, C.E.N., European Committee for Standardization.

[17] Italian Ministry of Infrastructures. Nuove norme tecniche per le costruzioni e relative istruzioni, D.M.14-01-2008 and Circolare 02-02-2009. n. 617/C.S.LL.PP.

[18] Stuani, E, Iurcotta E, Genta U. Manuale tecnico del geometra e del perito agrario, Signorelli, Milano, Italy 1967 (in Italian).

[19] Santarella L. Il cemento armato. Le applicazioni alle costruzioni civili ed industriali, Hoepli, Milano, Italy; 1975 (in Italian).

[20] CNR-DT 200/2013. Guide for the design and construction of externally bonded FRP systems for strengthening existing structures: materials, RC and PC structures, masonry structures, National Research Council, Rome.

[21] Mazza F, Vulcano A, Mazza M. Nonlinear dynamic response of rc buildings with different base-isolation systems subjected to horizontal and vertical components of near-fault ground motions. Open Constr Build Technol J 2012;6:373–83.

[22] CNR-DT 212/2013. Instructions for seismic safety assessment of existing buildings, National Research Council, Rome.

[23] Zhu L, Elwood KJ, Haukaas T. Classification and seismic safety evaluation of existing reinforced concrete columns. J Struct Eng ASCE 2007;133(9):1316–30.

[24] Haselton CB, Liel AB, Lange ST, Deierlein GG. Beam-column element model calibrated for predicting flexural response leading to global collapse of RC frame buildings. 2007. p. 3.

[25] Sezen H, Moehle J. Shear strength for lightly reinforced concrete columns. J Struct Eng ASCE 2004;130(11):1692–703.

[26] Hegger J, Sherif A, Roeser W. Nonseismic design of beam-column joints. ACI Struct J 2003;100(5):654–64.

[27] Kim J, LaFave JM, Song J. Joint shear behaviour of reinforced concrete beam-column connections. Mag Concr Res 2009;61(2):119–32.

[28] Mander JB, Priestley MJN, Park R. Theoretical stress-strain model for confined concrete. J Struct Eng ASCE 1988;114(8):1804–26.

[29] Martinez-Rueda JE, Elnashai AS. Confined concrete model under cyclic load. Mater Struct 1997;30(197):139–47.

[30] Gasparini D, Vanmarcke E. Simulated earthquake motions compatible with prescribed response spectra. U.S.A.: Massachusetts Institute of Technology, Dept. of Civil Eng.; 1976.